INSTITUTE OF PHYSICS PUBLISHING MODELLING AND SIMULATION IN MATERIALS SCIENCE AND ENGINEERING

Modelling Simul. Mater. Sci. Eng. **13** (2005) 759–769 doi:10.1088/0965-0393/13/5/009

Application of various FLD modelling approaches

D Banabic[1], H Aretz[2], L Paraianu[1] and P Jurco[1]

[1] Technical University of Cluj-Napoca, C. Daicoviciu 15, 3400 Cluj-Napoca, Romania
[2] LASSO Ingenieurgesellschaft mbH, Markomannenstrasse 11,
70771 Leinfelden-Echterdingen, Germany

E-mail: dorel.banabic@tcm.utcluj.ro

Received 2 September 2004, in final form 24 May 2005
Published 1 July 2005
Online at stacks.iop.org/MSMSE/13/759

Abstract

This paper focuses on a comparison between different modelling approaches to predict the forming limit diagram (FLD) for sheet metal forming under a linear strain path using the recently introduced orthotropic yield criterion BBC2003 (Banabic D *et al* 2005 *Int. J. Plasticity* **21** 493–512). The FLD models considered here are a finite element based approach, the well known Marciniak–Kuczyński model, the modified maximum force criterion according to Hora *et al* (1996 *Proc. Numisheet'96 Conf. (Dearborn/Michigan)* pp 252–6), Swift's diffuse (Swift H W 1952 *J. Mech. Phys. Solids* **1** 1–18) and Hill's classical localized necking approach (Hill R 1952 *J. Mech. Phys. Solids* **1** 19–30). The FLD of an AA5182-O aluminium sheet alloy has been determined experimentally in order to quantify the predictive capabilities of the models mentioned above.

1. Introduction and objectives

1.1. Introduction

Formability of sheet metals is at present characterized by the *forming limit diagram* (FLD, sometimes also denoted by FLD_{ε}) introduced in the 1960s by Keeler and Backofen [13] and Goodwin [6]. The experimental technique to determine the FLD involves subjecting specimens of the considered sheet metal to different in-plane strain states, e.g. by simple tensile testing or stretching over a hemispherical punch. The FLD represents a plot of major and minor limiting in-plane strain couples corresponding to the occurrence of visible defects in the sheet metal like necking and fracture. In practice, the necking FLD is of major interest because (among other reasons), necking usually occurs prior to fracture in ductile metals. The limiting strains in the FLD corresponding to necking describe more or less a curve called the 'forming limit curve' (FLC) [17, p 70]. (In practice, however, a scatter band rather than a curve is obtained.) The maximum FLC is obtained by pre-straining the sheet in uniaxial tension followed by equibiaxial stretching [8, 11, p 322, 18]. This indicates that maximum forming could be brought to complex parts made of sheets if the material is first locally stretched in uniaxial tension followed by biaxial stretching.

In sheet forming analysis a distinction is made between *diffuse* and *localized* necking. In industrial stampings, the maximum allowable straining is determined by localized rather than by diffuse necking [18]. Following Hosford and Caddell [11, p 309] *diffuse* necking is accompanied by contraction strains in both the width and the thickness directions of the sheet. The whole neck develops gradually and considerable extension is still possible after the onset of diffuse necking. Finally, a condition will be reached where a sharp *localized* neck can form. Its width is of the order of the sheet thickness. In a localized neck the strain along the necking band is zero and, assuming volume constancy, the thickness strain is exclusively provided by the remaining in-plane strain. According to Barlat [4], localized necking corresponds to exceeding a critical thickness strain. Hence, the limiting strains of the material under biaxial loading are associated with its thinning resistance [4].

The FLD of metallic sheets is influenced by various factors. A comprehensive overview may be found in [2, pp 198–203, 16, pp 213–33, 17, pp 75–80]. Because of space limitations, these influencing factors are not repeated here. Details on experimental aspects of sheet FLDs may also be found in [2].

1.2. Objectives

In this paper, a finite element based approach, the well known Marciniak–Kuczyński (M–K) model, the modified maximum force criterion (MMFC) according to Hora *et al* [9], Swift's diffuse [19] and Hill's classical localized necking approaches [7] are utilized to simulate the FLD of an AA5182-O aluminium sheet alloy using the recently introduced orthotropic yield criterion BBC2003 [3]. In order to quantify the predictive capability of the individual modelling approaches, their predictions are compared to an experimentally determined FLD of the considered aluminium alloy sheet metal.

2. Theoretical framework

2.1. BBC2003 yield criterion

The sheet metal is assumed to behave as a plastically orthotropic membrane under plane stress conditions. In this paper isotropic hardening is assumed and the rate-independent plasticity theory along with the associative flow-rule is applied. The yield function Φ is given by

$$\Phi(\sigma_{ij}, Y_{\text{ref}}) = \bar{\sigma}(\sigma_{ij}) - Y_{\text{ref}} = 0, \tag{1}$$

where $\bar{\sigma}(\sigma_{ij})$ is the equivalent stress according to the BBC2003 yield criterion, see below. Y_{ref} is a reference yield stress and σ_{ij}, $i, j = 1, 2$, are components of the plane stress tensor related to an orthonormal basis coinciding with the following axes of plastic orthotropy: 1—rolling direction (RD), 2—transverse direction (TD) and 3—normal direction (ND).

Following [3], the equivalent stress used in equation (1) is defined as

$$\bar{\sigma}(a, M, N, P, Q, R, S, T, k, \sigma_{ij}) = [a \cdot (\Gamma + \Psi)^{2k} + a \cdot (\Gamma - \Psi)^{2k} + (1 - a) \cdot (2\Lambda)^{2k}]^{1/2k}, \tag{2}$$

where $k \in \mathbb{N}^{\geqslant 1}$ and $0 \leqslant a \leqslant 1$ are material parameters while Γ, Ψ and Λ are defined as

$$\begin{aligned} \Gamma &= \frac{\sigma_{11} + M\sigma_{22}}{2}, \\ \Psi &= \sqrt{\frac{(N\sigma_{11} - P\sigma_{22})^2}{4} + Q^2\sigma_{12}\sigma_{21}}, \\ \Lambda &= \sqrt{\frac{(R\sigma_{11} - S\sigma_{22})^2}{4} + T^2\sigma_{12}\sigma_{21}}. \end{aligned} \tag{3}$$

The coefficients M, N, P, Q, R, S and T involved in equation (3) are also material dependent parameters. The choice of the integer exponent k is motivated by the pioneering work of Hosford *et al* [10–12]: $k = 3$ for bcc materials, and $k = 4$ for fcc materials.

In a numerical identification procedure the parameters M, N, P, Q, R, S, T and a are calculated by forcing the constitutive equations associated with the BBC2003 yield criterion to reproduce the following experimental input data.

- The uniaxial yield stresses associated with the directions defined by the orientation angles, 0°, 45° and 90°, measured from RD. They are denoted here as Y_0, Y_{45} and Y_{90}.
- The coefficients of uniaxial plastic anisotropy associated with the directions defined by 0°, 45° and 90° angles measured from RD. They are denoted here as r_0, r_{45} and r_{90}.
- The equibiaxial yield stress, Y_b, associated with RD and TD.
- The coefficient of equibiaxial plastic anisotropy [5], r_b, associated with RD and TD.

In [3], a Newton solver has been presented to calculate the anisotropy parameters. The same solver has been applied in the present work.

2.2. *Marciniak–Kuczyński model*

In industrial stampings, the maximum allowable straining is determined by localized necking rather than by diffuse necking [18]. Usually, the localized neck develops normal to the maximum principal in-plane stress [17, p 72]. However, as was pointed out by Marciniak *et al* [17, p 72], the development of a localized neck in a sheet metal subjected to biaxial stretching is impossible since there is no direction of zero extension. However, since localized necking in biaxial stretching is observed in practice, a pre-existing imperfection has to be introduced in the necking model to capture this effect. In the strain localization model proposed by Marciniak and co-workers [14, 15] the imperfection is introduced by means of a small thickness inhomogeneity. Figure 1 shows two neighbouring regions of the sheet: region 'a' has the nominal initial thickness t_0^{a}, while the 'groove' (region 'b') is slightly thinner (initial thickness t_0^{b}). The ratio of the initial thicknesses is used to define the inhomogeneity coefficient

$$f_0 = \frac{t_0^{\mathrm{b}}}{t_0^{\mathrm{a}}}. \tag{4}$$

In the present work, $f_0 = 0.98$ has been applied.

The following relationships express the compatibility of the strain increments corresponding to region 'a' and region 'b', respectively:

$$\Delta\varepsilon_{22}^{\mathrm{b}} = \Delta\varepsilon_{22}^{\mathrm{a}}, \qquad \Delta\varepsilon_{tt}^{\mathrm{b}} = \Delta\varepsilon_{tt}^{\mathrm{a}}. \tag{5}$$

With respect to figure 1, the mechanical equilibrium at the interface is expressed by the equations

$$\begin{aligned} \sigma_{nn}^{\mathrm{a}} \cdot t^{\mathrm{a}} &= \sigma_{nn}^{\mathrm{b}} \cdot t^{\mathrm{b}}, \\ \sigma_{tn}^{\mathrm{a}} \cdot t^{\mathrm{a}} &= \sigma_{tn}^{\mathrm{b}} \cdot t^{\mathrm{b}}. \end{aligned} \tag{6}$$

The ratio of the strain increments in region 'a' is expressed as follows

$$\rho = \frac{\Delta\varepsilon_{22}^{\mathrm{a}}}{\Delta\varepsilon_{11}^{\mathrm{a}}}. \tag{7}$$

The value of the principal strain $\varepsilon_{11}^{\mathrm{a}}$ in region 'a' corresponding to non-significant straining of this region as compared to region 'b' (the straining being localized in region 'b') represents the limit strain $\varepsilon_{11}^{\mathrm{a*}}$ (figure 2). By our experience, localized necking occurs when the increment of the equivalent strain in region 'b' is seven times larger than in region 'a'.

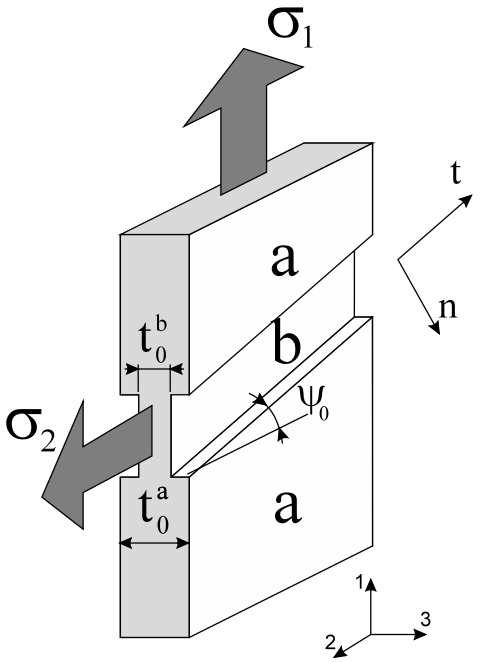

Figure 1. The M–K model. The transverse direction t is parallel to the groove, while the ND n is perpendicular to it.

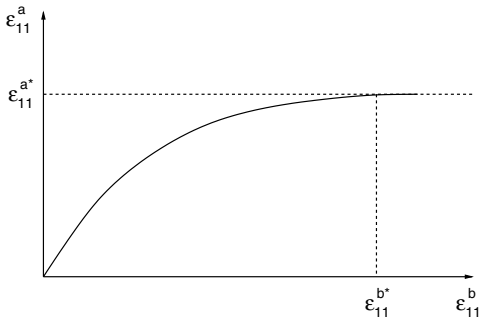

Figure 2. On the dependence ε_{11}^{a}–ε_{11}^{b}.

This strain together with the second principal strain ε_{22}^{a*} in region 'a', defines a point belonging to the FLD. Assuming different strain ratios $\rho = \Delta\varepsilon_{22}/\Delta\varepsilon_{11}$, one obtains different points of the FLD. By scrolling the range $0 < \rho < 1$, one gets the FLD for biaxial tension ($\varepsilon_{11} > 0$, $\varepsilon_{22} > 0$). In this domain, the orientation of the geometrical non-homogeneity with respect to the principal directions is assumed to be the same during the entire forming process.

2.3. Necking models according to Hill, Swift and Hora

In each of the FLD models in the present section, the following assumptions are made.

- The material under consideration is assumed to be rigid-plastic. Hence for the strains and strain rates $\varepsilon_{ij} = \varepsilon_{ij}^{pl}$ and $\dot{\varepsilon}_{ij} = \dot{\varepsilon}_{ij}^{pl}$, respectively. (The superscript $(\cdot)^{pl}$ stands for 'plastic'.)

- A principal plane stress state is assumed, i.e. σ_{11}, σ_{22} are the only non-zero stresses acting in the sheet plane. σ_{11}, σ_{22} are the major and minor in-plane principal stresses, respectively, i.e. $\sigma_{11} \geqslant \sigma_{22}$. This results in a principal strain rate state whereby $\dot{\varepsilon}_{11}$, $\dot{\varepsilon}_{22}$, $\dot{\varepsilon}_{33}$ are the only non-zero strain rates. Damage is excluded. Thus, the volume of the sheet material remains constant during plastic deformation, i.e. $\dot{\varepsilon}_{33} = -\dot{\varepsilon}_{11} - \dot{\varepsilon}_{22}$. $\dot{\varepsilon}_{11}, \dot{\varepsilon}_{22}$ are the major and minor principal in-plane strain rates, respectively, whereby $\dot{\varepsilon}_{11} \geqslant \dot{\varepsilon}_{22}$.
- The sheet deforms under proportional straining (linear strain path), i.e. $\dot{\varepsilon}_{11}/\dot{\varepsilon}_{22} = \varepsilon_{11}/\varepsilon_{22} = \text{constant}$.
- Isotropic hardening is considered.
- The anisotropy axes coincide with the principal strain and stress axes. (The case where the anisotropy axes do *not* coincide with the principal strain and stress axes has not been investigated in the present work since the mentioned necking models have been applied in their classical formulation.)

In order to describe the left-hand side of the FLD, i.e. the negative minor in-plane strain region, the localized necking criterion developed by Hill [7] is frequently used. It is given by

$$\frac{\mathrm{d}\sigma_{11}}{\mathrm{d}\varepsilon_{11}} = \sigma_{11} \cdot (1 + \beta), \qquad \beta := \frac{\dot{\varepsilon}_{22}}{\dot{\varepsilon}_{11}} = \text{constant}. \tag{8}$$

Localized necking takes place if the equality is fulfilled. Depending on the hardening law, the Hill necking criterion predicts a more or less straight line in the FLD.

In order to model the right-hand side of the FLD, the Swift necking criterion [19] can be used which states that diffuse necking occurs if

$$\frac{\mathrm{d}\sigma_{11}}{\mathrm{d}\varepsilon_{11}} = \sigma_{11} \tag{9}$$

holds. However, the Swift necking criterion is often too conservative and it underestimates the experimentally observed forming limit strains significantly.

Hora *et al* [9] intended to improve Swift's criterion by taking into account the experimentally confirmed fact, that the onset of necking depends significantly on the strain ratio β, defined here as $\beta := \dot{\varepsilon}_{22}/\dot{\varepsilon}_{11}$. (For proportional straining $\beta = \dot{\varepsilon}_{22}/\dot{\varepsilon}_{11} = \varepsilon_{22}/\varepsilon_{11} = \text{constant}$.) The 'MMFC' proposed to Hora *et al* [9] reads as

$$\frac{\partial\sigma_{11}}{\partial\varepsilon_{11}} + \frac{\partial\sigma_{11}}{\partial\beta} \cdot \frac{\partial\beta}{\partial\varepsilon_{11}} = \sigma_{11}, \qquad \beta := \frac{\dot{\varepsilon}_{22}}{\dot{\varepsilon}_{11}} = \text{constant}. \tag{10}$$

It was shown by Aretz [1], that the computational framework for each of the three necking models mentioned may be formulated in a uniform manner. The same framework is applied in the present work.

An important drawback of the MMFC is the fact that it contains a singularity that emerges if the yield locus contains straight line segments [1]. A comprehensive discussion of this singularity problem is found in [1]. Due to the singularity problem, the left-hand side of the FLD is predicted by means of the Hill localized necking model, shown later in this paper, although the MMFC is, basically, able to predict the left-hand side as well. (One should however, *not* conclude that the singularity emerges always in the left-hand side of the FLD. In general, the location of the singularity depends on the yield locus and can emerge on the left- or right-hand side of the FLD.)

2.4. Finite element based approach for modelling of localized necking

The process of strain localization has been simulated using the commercial FEM code ABAQUS/Standard. The BBC2003 yield criterion has been implemented as a user-defined

material in the ABAQUS user subroutine UMAT. The elasto-plastic constitutive law has the following expression.

$$\{\boldsymbol{\delta\sigma}\} = [\boldsymbol{C}^{\mathrm{ep}}] \cdot \{\boldsymbol{\delta\varepsilon}\}, \tag{11}$$

where $\{\boldsymbol{\delta\sigma}\} = [\delta\sigma_{11}, \delta\sigma_{22}, \delta\sigma_{12}]^{\mathrm{T}}$ and $\{\boldsymbol{\delta\varepsilon}\} = [\delta\varepsilon_{11}, \delta\varepsilon_{22}, 2\delta\varepsilon_{12}]^{\mathrm{T}}$ are column-vectors containing the perturbations of the stress and strain tensors, respectively. $[\boldsymbol{C}^{\mathrm{ep}}]$ is the consistent elasto-plastic tangent stiffness matrix calculated using the following matrix formula:

$$[\boldsymbol{C}^{\mathrm{ep}}] = [\boldsymbol{Q}] - \frac{([\boldsymbol{Q}] \cdot \{\boldsymbol{g}\}) \cdot ([\boldsymbol{Q}] \cdot \{\boldsymbol{g}\})^{\mathrm{T}}}{\{\boldsymbol{g}\}^{\mathrm{T}} \cdot [\boldsymbol{Q}] \cdot \{\boldsymbol{g}\} + (\partial Y_{\mathrm{ref}}/\partial\bar{\varepsilon})}, \tag{12}$$

where

$$[\boldsymbol{C}^{\mathrm{ep}}] = \begin{bmatrix} C^{\mathrm{ep}}_{1111} & C^{\mathrm{ep}}_{1122} & C^{\mathrm{ep}}_{1112} \\ & C^{\mathrm{ep}}_{2222} & C^{\mathrm{ep}}_{2212} \\ \text{symm.} & & C^{\mathrm{ep}}_{1212} \end{bmatrix}, \tag{13}$$

$$\{\boldsymbol{g}\} = \left[\frac{\partial\Phi}{\partial\sigma_{11}}, \frac{\partial\Phi}{\partial\sigma_{22}}, 2\frac{\partial\Phi}{\partial\sigma_{12}}\right]^{\mathrm{T}}, \tag{14}$$

$$[\boldsymbol{Q}] = ([\boldsymbol{C}^{\mathrm{e}}]^{-1} + \Delta\bar{\varepsilon} \cdot [\boldsymbol{M}])^{-1}, \tag{15}$$

$$[\boldsymbol{M}] = \begin{bmatrix} \dfrac{\partial^2\Phi}{\partial\sigma_{11}^2} & \dfrac{\partial^2\Phi}{\partial\sigma_{11}\partial\sigma_{22}} & 2\dfrac{\partial^2\Phi}{\partial\sigma_{11}\sigma_{12}} \\ & \dfrac{\partial^2\Phi}{\partial\sigma_{22}^2} & 2\dfrac{\partial^2\Phi}{\partial\sigma_{22}\sigma_{12}} \\ \text{symm.} & & 2\left(\dfrac{\partial^2\Phi}{\partial\sigma_{12}^2} + \dfrac{\partial^2\Phi}{\partial\sigma_{12}\sigma_{21}}\right) \end{bmatrix}, \tag{16}$$

$$[\boldsymbol{C}^{\mathrm{e}}] = \frac{E}{1-\nu^2} \cdot \begin{bmatrix} 1 & \nu & 0 \\ \nu & 1 & 0 \\ 0 & 0 & (1-\nu/2) \end{bmatrix}. \tag{17}$$

$\{\boldsymbol{g}\}$ is the vector of the yield surface gradient, $\partial Y_{\mathrm{ref}}/\partial\bar{\varepsilon}$ the strain-hardening modulus associated with the applied hardening curve, $\Delta\bar{\varepsilon}$ the increment of equivalent plastic strain, $[\boldsymbol{M}]$ the matrix of the second order yield surface gradient and $[\boldsymbol{C}^{\mathrm{e}}]$ the classical elastic modulus (containing the Young's modulus E and the Poisson's ratio ν). The orthotropy axes have been defined as follows: the sheet's rolling direction is assigned perpendicular to the groove while the sheet transverse has been assigned parallel to the groove.

The second role of the UMAT routine is to detect the strain localization. Motivated by the M–K approach, two reference elements have been chosen for this purpose. One of them is placed in region 'a' far from the groove region 'b'. The second reference element is located in the middle of region 'b'. Each time the UMAT routine is called for these elements, it will store the current values of the strain rates in two static variables. The FEM simulation terminates when the strain rate associated with the reference element placed in region 'a' is seven times larger than the strain increment associated with the element placed in region 'b'. The corresponding point belonging to the FLD is defined by the values of the principal logarithmic strains calculated at the end of the previous time increment for the reference element placed in region 'a'.

The above procedure has been repeated for six different displacement ratios along the 1- and 2-axis. The FLC is represented by a linear interpolation of the discrete points calculated

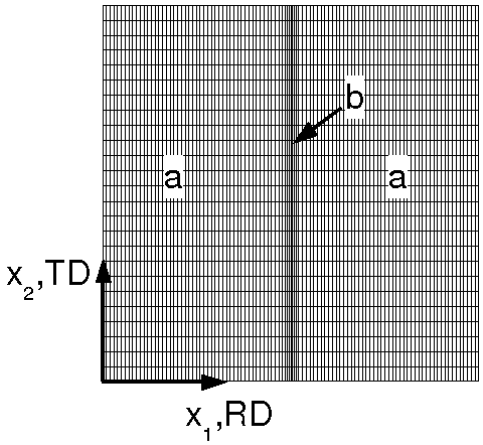

Figure 3. Initial geometry of the finite element mesh. Region 'a' denotes the homogeneous region while region 'b' denotes the groove. 'RD' means 'rolling direction' while 'TD' means 'transverse direction'.

Table 1. Material parameters of the aluminium alloy AA5182-O.

Y_0 (MPa)	Y_{45} (MPa)	Y_{90} (MPa)	Y_b (MPa)	Y_{ref} (MPa)	r_0	r_{45}	r_{90}	r_b	k
143.5	139.0	142.5	143.5	143.5	0.642	1.039	0.829	1.126	4

by ABAQUS. Figure 3 shows the initial finite element mesh used in the numerical simulations. Its dimensions are 25 : 25 conventional units. In order to represent the thickness imperfection area (region 'b'), a strip of 1 : 25 units has been located in the symmetry plane. The thickness in the finite elements that form the imperfection region is smaller than in the remaining elements. As seen in figure 3, the mesh is finer in region 'b' than in region 'a'. The utilized ABAQUS element type is 'M3D4' (4 node quadrilateral membrane).

So far, finite element solutions have been obtained for the positive minor in-plane strain regime, i.e. for the right-hand side of the FLD. A finite element based approach to model the left-hand side of the FLD is currently in progress.

3. Material characterization

The material under consideration is the aluminium alloy AA5182-O. The initial sheet thickness is 1.0 mm. The experimentally determined material data is given in table 1. In order to calibrate the yield function BBC2003, the following data has been selected as input data: Y_0, Y_{45}, Y_{90}, Y_b, r_0, r_{45}, r_{90}, r_b. The reference yield stress Y_{ref}, which can be chosen arbitrarily, has been set identical to Y_0. Table 2 displays the calculated anisotropy parameters for BBC2003. A Newton solver comprehensively described in [3] has been utilized for their numerical calculation. The equibiaxial data, Y_b and r_b, have been obtained from the cross-tensile test technique presented in [3].

Figures 4–6 display the BBC2003 predictions concerning directional r-values, yield stresses and yield surface. It may be seen that the yield function meets the experimental input data points exactly. Although not shown here it should be mentioned that BBC2003 also meets the experimental equibiaxial yield stress $Y_b = 143.5$ MPa, and the equibiaxial r-value, $r_b = 1.126$ exactly.

Table 2. Calculated BBC2003 anisotropy parameters for the AA5182-O material obtained by means of a Newton solver. The numbers are rounded to five digits for convenience.

M	*N*	*P*	*Q*	*R*	*S*	*T*	*a*
0.934 26	1.002 17	1.026 81	1.034 23	0.997 96	1.046 19	1.077 42	0.650 31

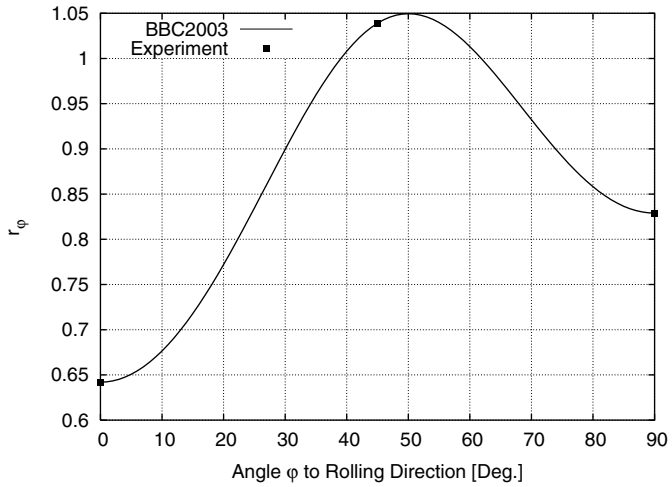

Figure 4. Comparison of experimental and predicted directional r-values for AA5182-O.

The assumed isotropic hardening behaviour is described by the Swift type function

$$Y_{\text{ref}}(\bar{\varepsilon}) = 585.2(0.004\,926 + \bar{\varepsilon})^{0.3232}\,\text{MPa} \tag{18}$$

obtained by curve fitting of the experimental hardening data of a uniaxial tensile test of a specimen with orientation parallel to the original RD.

4. Comparison between predicted and experimental forming limits

The predicted and experimentally determined FLD data are displayed in figure 7. Note that *logarithmic* strains are displayed in figure 7. It can easily be seen that the Swift–Hill and Hora–Hill approaches overestimate considerably the experimental necking FLD throughout the whole minor in-plane strain region. The results of the M–K model and the finite element approach are very close to each other, confirming the validity of the M–K model. In contrast to the FEM approach, the M–K model predicts a shift in the minimum of the FLC to the right. This shift could not be captured by the FEM approach. This is possibly due to the fact that, in contrast to the applied M–K model, the groove is not allowed to rotate in the FEM approach. Both approaches underestimate the experimental necking FLD in the equibiaxial stress region while they overestimate the experimental necking FLD in the plane strain region and in the uniaxial tensile stress region.

An interesting aspect of the predicted FLDs is the fact that the Hora–Hill and the Swift–Hill approaches overestimate the experimental necking FLD as well as the predictions of the M–K model, and of the finite element based approach. This is unexpected in so far that the Swift and the Hora approaches are diffuse necking models and one would, therefore, expect the

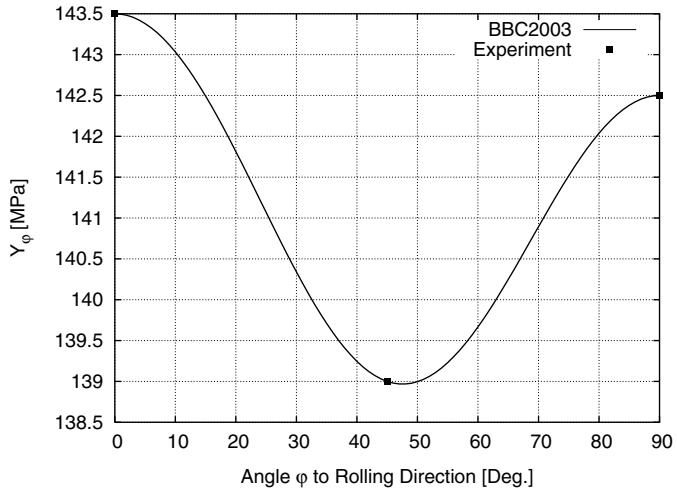

Figure 5. Comparison of experimental and predicted directional yield stresses for AA5182-O.

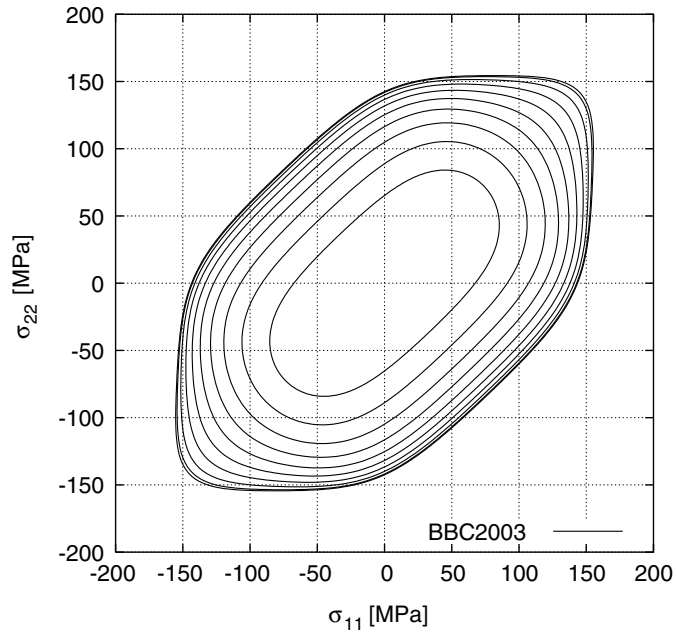

Figure 6. Predicted tri-component yield surface for AA5182-O. Displayed are contours in the σ_{11}–σ_{22}–σ_{12} stress space (with the σ_{12}-axis perpendicular to the paper plane). The calculated maximum in-plane shear yield stress is $Y_\tau = 75.841\,84$ MPa. The displayed contours are calculated for steps of $\Delta Y_\tau = 7.584\,184$ MPa.

predicted forming limit curve to lie below the one predicted by a localized necking model (such as the M–K model). Additionally, the Swift model is known to be too conservative in FLD prediction, but the contrary is observed in the present case (in accordance with the afore mentioned). One may speculate whether the predictive capabilities of these models will be improved if the major stress and strain axes, as well as the orthotropy axes, are not enforced to coincide. This is, however, beyond the scope of this work.

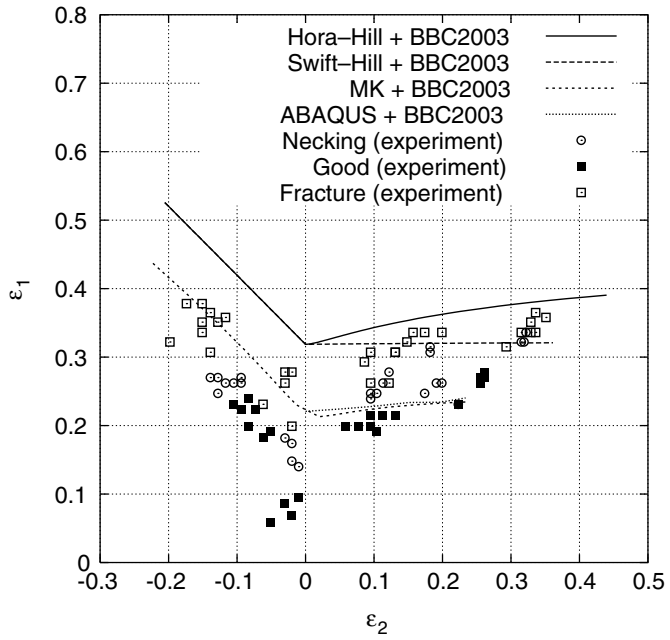

Figure 7. Predicted and experimental FLD.

5. Summary

In this paper, various localized and diffuse necking models have been applied to predict the FLD of an AA5182-O aluminium sheet alloy. The FLD models considered here are a finite element based approach, the well known M–K model, the MMFC according to Hora *et al* [9], Swift's diffuse [19] and Hill's classical localized necking approach [7] along with the recently introduced orthotropic yield criterion BBC2003 [3]. It has been shown that the results of the M–K model and the finite element based approach are very close to each other, confirming the validity of the M–K model. Both approaches agreed best with the experimental necking FLD. The remaining FLD models overestimated the experimental necking FLD considerably.

References

[1] Aretz H 2004 Numerical restrictions of the modified maximum force criterion for prediction of forming limits in sheet metal forming *Modelling Simul. Mater. Sci. Eng.* **12** 677–92
[2] Banabic D, Bunge H-J, Pöhlandt K and Tekkaya A E 2000 *Formability of Metallic Materials* (Berlin: Springer)
[3] Banabic D, Aretz H, Comsa D S and Paraianu L 2005 An improved analytical description of orthotropy in metallic sheets *Int. J. Plasticity* **21** 493–512
[4] Barlat F 1987 Crystallographic texture, anisotropic yield surfaces and forming limits of sheet metals *Mater. Sci. Eng.* **91** 55–72
[5] Barlat F, Brem J C, Yoon J W, Chung K, Dick R E, Choi S-H, Pourboghrat F, Chu E and Lege D J 2003 Plane stress yield function for aluminium alloy sheets—part 1: theory *Int. J. Plasticity* **19** 1297—319
[6] Goodwin G M 1968 Application of strain analysis to sheet metal forming problems in the press shop *La Metallurgia Italiana* **8** 767–74
[7] Hill R 1952 On discontinous plastic states, with special reference to localized necking in thin sheets *J. Mech. Phys. Solids* **1** 19–30

[8] Hiwatashi S, Van Bael A, Van Houtte P and Teodosiu C 1998 Prediction of forming limit strains under strain-path changes: application of an anisotropic model based on texture and dislocation structure *Int. J. Plasticity* **14** 647–69
[9] Hora P, Tong L and Reissner J 1996 A prediction method for ductile sheet metal failure in FE-simulation *Proc. Numisheet'96 Conf. (Dearborn/Michigan)* pp 252–6
[10] Hosford W F 1972 A generalized isotropic yield criterion *J. Appl. Mech.* **39** 607–9
[11] Hosford W F and Caddell R M 1993 *Metal Forming—Mechanics and Metallurgy* 2nd edn (Englewood Cliffs, NJ: Prentice-Hall)
[12] Hosford W F 1993 *The Mechanics of Crystals and Textured Polycrystals* (Oxford Science Publications)
[13] Keeler S P and Backofen W A 1963 Plastic instability and fracture in sheets stretched over rigid punchs *Trans. ASM* **56** 25–48
[14] Marciniak Z and Kuczyński K 1967 Limit strains in the process of stretch-forming sheet metal *Int. J. Mech. Sci.* **9** 609–20
[15] Marciniak Z, Kuczyński K and Pokora T 1973 Influence of the plastic properties of a material on the forming limit diagram for sheet metal in tension *Int. J. Mech. Sci.* **15** 789–805
[16] Marciniak Z 1978 Instability processes *Mechanics of Sheet Metal Forming* ed D Koistinen and N-M Wang (New York, London: Plenum)
[17] Marciniak Z, Duncan J L and Hu S J 2002 *Mechanics of Sheet Metal Forming* 2nd edn (Oxford: Butterworth-Heinemann)
[18] Barata da Rocha A, Barlat F and Jalinier J M 1984–1985 Prediction of the forming limit diagrams of anisotropic sheets in linear and non-linear loading *Mater. Sci. Eng.* **68** 151–64
[19] Swift H W 1952 Plastic instability under plane stress *J. Mech. Phys. Solids* **1** 1–18